

Communication

# Oscillatory Mechanism of $\alpha$ -Fe(N) $\leftrightarrow$ $\gamma'$ -Fe<sub>4</sub>N Phase Transformations during Nanocrystalline Iron Nitriding

Walerian Arabczyk, Katarzyna Skulmowska, Rafał Pelka \*  and Zofia Lendzion-Bieluń

Department of Inorganic Chemical Technology and Environment Engineering, Faculty of Chemical Technology and Engineering, West Pomeranian University of Technology in Szczecin, Piastów Ave. 42, 71-065 Szczecin, Poland; walerian.arabczyk@zut.edu.pl (W.A.); katarzyna.skulmowska@zut.edu.pl (K.S.); Zofia.Lendzion-Bielun@zut.edu.pl (Z.L.-B.)

\* Correspondence: rpelka@zut.edu.pl

**Abstract:** The kinetics of nanocrystalline  $\alpha$ -iron nitriding to  $\gamma'$ -iron nitride in an ammonia atmosphere was studied at 598–648 K and at atmospheric pressure. Oscillatory changes in nitriding reaction rates depending on nitrogen concentration in a solid sample were observed. This phenomenon was explained by a gradual change in the iron active surface coverage degree, with nitrogen resulting from a gradual change in the free enthalpy of nitrogen segregation. The  $\alpha$ -Fe(N) nanocrystallites' transformation into  $\gamma'$ -Fe<sub>4</sub>N went through six metastable FeN<sub>x</sub> states. The continuous function proposed by Fowler and Guggenheim was modified to a stepwise variable function.

**Keywords:** nanocrystalline iron; nitriding process; kinetics; oscillations; ammonia



**Citation:** Arabczyk, W.; Skulmowska, K.; Pelka, R.; Lendzion-Bieluń, Z. Oscillatory Mechanism of  $\alpha$ -Fe(N)  $\leftrightarrow$   $\gamma'$ -Fe<sub>4</sub>N Phase Transformations during Nanocrystalline Iron Nitriding. *Materials* **2022**, *15*, 1006. <https://doi.org/10.3390/ma15031006>

Academic Editor: Francisca G. Caballero

Received: 23 November 2021

Accepted: 25 January 2022

Published: 27 January 2022

**Publisher's Note:** MDPI stays neutral with regard to jurisdictional claims in published maps and institutional affiliations.



**Copyright:** © 2022 by the authors. Licensee MDPI, Basel, Switzerland. This article is an open access article distributed under the terms and conditions of the Creative Commons Attribution (CC BY) license (<https://creativecommons.org/licenses/by/4.0/>).

## 1. Introduction

Due to the practical applications of the iron and steel nitriding process, it was studied in the presence of coarse-crystalline iron and thin iron foils [1–5]. During these studies, Grabke, among others, observed that the surface chemical reaction is a rate-limiting step only in the initial phase of the process [3,4]. Later in the process, the diffusion of substrate through the product layer limits the nitriding rate.

In order to understand the nitriding mechanism, a simpler model system was used, in which nanocrystalline iron reacts with gaseous ammonia. In the case of nitriding of nanocrystalline iron, the effect of the diffusion of substances through the product layer on the process rate may be neglected due to the small size of nanoparticles and, thus, short (compared to coarse-crystalline materials) mass transport paths. In the process of nitriding of nanocrystalline iron there are two parallel reactions: the iron nitriding reaction, and catalytic decomposition of ammonia. The kinetics of the nanocrystalline iron nitriding process are presented in many other works [6–10]. Nitriding processes were conducted in the kinetic region at the nitriding potential of the gas phase, defined as  $P = p_{\text{NH}_3} / p_{\text{H}_2}^{3/2}$ —much higher than the steady state potential ( $P^{\text{eq}}$ )—at temperatures (T) above 673 K [7]. Smaller nanocrystallites of iron achieved the nitrogen critical concentration in their volume ( $X_{\text{N}}^{\text{cri}}$ ) faster than larger ones [11]. Consequently, it was observed that nanocrystallites underwent the phase transformation according to their sizes, ranging from the smallest up to the largest. The phase transformation in a single iron nanocrystallite occurs throughout its volume. A model of reaction in the nanocrystalline materials–gas phase system in the adsorption area was developed [12], where it was stated that the dissociative adsorption rate of the gas phase on the nanocrystallite surface limited the rate of chemical reaction.

In the isothermal processes of nitriding of nanocrystalline iron, as well as reduction of nanocrystalline iron nitrides using ammonia–hydrogen gas mixtures at a determined nitriding potential, stationary states occurred [13,14]. A hysteresis was observed for the dependence of the nitriding degree on nitriding potential [13–17]. It was also found that the chemical potentials of nitrogen occurring in all three parts of the system—in the

gaseous phase, on the iron nanocrystallite surface and in nanocrystallite volume — equaled one another in the stationary states, i.e., chemical equilibrium was established [16,18,19]. There was only a reaction of catalytic ammonia decomposition [20]. The minimum nitriding potentials required to initiate nitriding of nanocrystalline iron and reduction of nanocrystalline nitrides are the linear functions of nanocrystallite sizes [8,18,19,21]. Phase transformation of nanocrystallites in close-to-equilibrium states takes place in the entire volume of nanocrystallites according to their sizes, starting from the largest down to the smallest [16,22]. Based on theoretical calculations concerning thermodynamic parameters, it was found that such an order of nanocrystallite transformation occurred in the nanocrystalline iron nitriding process as well as in the reduction of nanocrystalline iron nitrides [18,19]. In the nanocrystalline iron nitriding process with ammonia–hydrogen mixtures, two solid phases occur simultaneously at the determined nitriding potential, and three solid phases in the wide ranges of nitriding potential occur simultaneously in the process of reducing the nanocrystalline  $\epsilon$  iron nitrides [15,23]. The Lehrer diagram does not explain the above-mentioned phenomena taking place in a system of nanocrystalline iron, ammonia, and hydrogen [24]. In order to describe these phenomena, an additional intensive parameter—the size of nanocrystallites—was introduced into the extended Gibbs phase rule [19].

The oscillatory kinetics of heterogeneous reactions have already been observed for systems involving phenomena on the surface of the solid phase [25–41]. It has been found that oscillatory states are caused by periodic variations in the degree of catalysts' surface coverage. Saraev et al. [42] observed oscillatory phenomena in solid-phase–gas-phase reaction systems with phase transformation of a solid substrate in the surface layer (a range of several dozens of atomic layers). As a result of detailed kinetic studies of the nitride reduction process, we observed oscillatory changes in the rate of the reduction reaction of iron  $\gamma'$ -Fe<sub>4</sub>N iron nitride to  $\alpha$ -iron [43]. The observed oscillatory phenomenon has been explained by a gradual variation in the free enthalpy of nitrogen segregation.

It can be concluded that the above phenomena are not observed in coarse-crystalline materials with a negligible specific surface, where the diffusion rate of the substrate through the product layer limits the rate of chemical reaction. In the case of these substances, the influence of surface reactions is not taken into account precisely because of the low value of the specific surface area. In the case of nanocrystalline substances, the share of surface and surface reactions is significant. Then, the surface energy plays an important role, and surface phenomena contribute to the free enthalpy of the whole chemical process. The transformation depends on the balance of both surface energy and that related to the volume of nanocrystallites. Thus, the aim of this work was to explain the phenomenon of the periodicity of chemical reaction rates in the case of nanocrystalline materials, and nanocrystalline iron nitriding with ammonia was used as an example of the system under study.

## 2. Materials and Methods

An industrial iron catalyst for ammonia synthesis—KM1R (pre-reduced form containing nanocrystalline iron doped with hardly reducible oxides of aluminum (3.3 wt.%), calcium (2.8 wt.%), and potassium (0.65 wt.%))—was used in the study. The average size of iron nanocrystallites prior to the nitriding process, as determined by X-ray diffraction (Rietveld method), was 45 nm. The specific surface area of the catalyst, as determined by the thermal desorption method, was 12 m<sup>2</sup>/g [44]. Nitriding reaction rate measurements were conducted in a differential tubular reactor with both a thermogravimetric measuring system and a hydrogen analyzer. A solid sample of 1 g was placed in the form of a single layer of grains (1.0–1.2 mm) in a platinum reactor basket suspended on the arm of a thermobalance. Ammonia (99.98%) and hydrogen (99.999%) were applied. The description of the installation is presented elsewhere [2]. During the exchange of hydrogen (present in the reactor) for ammonia, the composition of the gas phase in the two-component system was changing. Model calculations of changes in the composition of the gas phase in the

reactor reaction volume were performed, taking into account the simplified differential mass balance equation of the reactor with perfect mixing:

$$-\frac{dX}{dt} = \frac{F_0(X_i - X)}{U} \quad (1)$$

where  $X_i$  is the concentration (mol/mol) (feed stream),  $F_0$  is the molar flow rate (mol/s),  $U$  is the total number of moles in the reactor volume, in which the reaction takes place, and  $t$  is the time (s).

The value of  $F_0$  was 0.00015 mol/s. By modeling Equation (1) with the experimental results, a value of  $U = 0.008$  mol was determined, corresponding to a reaction volume of 180 cm<sup>3</sup>.

Figure 1 contains the dependence of hydrogen concentration on time (the so-called “elution curve”) and a comparison of the results calculated with the experimental data. Based on the compatibility of the model and experimental results for hydrogen concentration measurements performed over and under the catalyst sample basket, it was found that under the experimental conditions in the reaction volume there was a state close to an ideal gas-phase mixing. The iron catalyst was subjected to a polythermal hydrogen reduction process, with temperature increasing from room temperature to 773 K at a rate of 0.24 K/s. The sample was reduced at 773 K until a constant mass was obtained. Selected measurement results concerning nanocrystalline iron nitriding with ammonia carried out isothermally at 648, 623, and 598 K are presented in this publication. During the nitriding process, ammonia was dosed into the reactor, and a gradual change in the gas-phase composition took place from hydrogen—present in the reactor after the catalyst reduction process—to ammonia. The nitriding process was conducted at a variable nitriding potential up to the moment when a stationary state was established, during which the measured hydrogen concentration in the reactor was constant and the rate of the nitriding reaction was zero. The composition of samples of nitrided nanocrystalline iron depends on the nitriding potential and temperature [24,45]. Under these conditions, nanocrystallites undergo phase transformation in the order from the smallest to the largest.

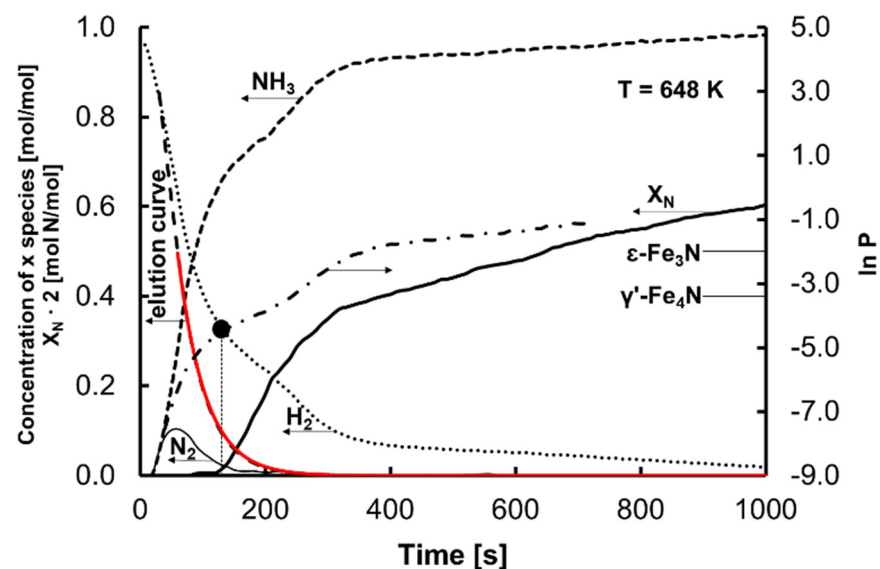


**Figure 1.** Dependence of the concentration of nitrogen in the nanocrystalline iron sample, the concentrations of hydrogen, ammonia, and nitrogen, and the nitriding potential on time for the nanocrystalline iron nitriding process (100% ammonia at the reactor inlet) at 648 K. The continuous red line shows the model results of the elution curve.

### 3. Results

Figure 1 shows an example of the dependence of the nitrogen concentration in the nanocrystalline iron sample, the concentrations of the individual components in the gaseous phase, and the change in nitriding potential on time for the nanocrystalline iron nitriding process at 648 K. Based on the results of thermogravimetric measurements and determination of hydrogen concentration in the gas phase, taking into account the mass balance of the reactor with perfect mixing, ammonia and nitrogen concentrations and nitriding potential were calculated at each process step [7].

Based on the computed composition of the gas phase, the minimal nitriding potential ( $P_0$ ), at which the phase transformation in the nitriding process of nanocrystalline iron begins, was determined. For each temperature in the nanocrystalline iron nitriding process, the smallest nanocrystallite reacts at a different nitriding potential. Based on the investigations of nanocrystalline iron nitriding processes in stationary states for the dependence of logarithms of nitriding potential on reciprocal temperature, the minimum nitriding potential of the smallest nanocrystallite for the temperature range 573–673 K can be described by the following equation [10,13,15–17,23]:

$$\ln P_0 = 18.3 + 8.91 \frac{1}{T} \quad (2)$$

In the nitriding process at a potential lower than the minimum nitriding potential at which the  $\gamma'$ -Fe<sub>4</sub>N phase is produced, samples of iron contained a small amount of nitrogen— $X_N = 0.004$  mol N/mol. At this stage of the nitriding process, an increase in the sample mass took place due to the adsorption of ammonia on the nanocrystalline iron surface and the formation of a solution of nitrogen in nanocrystalline iron, referred to as  $\alpha$ -Fe(N). Based on Equation (2), the minimum nitriding potential in the nitriding process of nanocrystalline iron at different reaction temperatures was calculated. For the dependence of hydrogen concentration on time (Figure 1), the value at which the hydrogen concentration corresponding to the nitriding potential ( $P_0$ ) was reached is marked with a black point.

### 4. Discussion

Based on the dependence of nitrogen concentration in the sample on the time of the nanocrystalline iron nitriding, the rates of this process were calculated as shown by time for temperatures of 648 and 598 K in Figure 2. For the dependence of the nanocrystalline iron nitriding rate on the time of the process, the occurrence of oscillatory reaction rate changes was observed. These oscillations were observed throughout the temperature range under investigation.

Making use of both the results presented in Figure 1 and the nitriding reaction rate shown in Figure 2, the dependence of the rates of the processes studied on nitrogen concentration in the sample were determined (Figure 3). The observed oscillations of the nitriding reaction rate depended on the nitrogen concentration in the iron.

The vertical continuous lines represent nitrogen concentrations at which the maximum nanocrystalline iron nitriding rate was observed. It was found that the six observed maxima in the nitriding process occurred at constant values of nitrogen concentration in iron, taking into account the measurement accuracy, at different temperatures.

Nanocrystalline iron nitriding processes were conducted under isothermal conditions with a variable nitriding potential. The transformation of the  $\alpha$ -Fe(N) phase to  $\gamma'$ -Fe<sub>4</sub>N starts with the minimum nitriding potential necessary to initiate the transformation of the smallest  $\alpha$ -Fe nanocrystallite into the  $\gamma'$  phase. The average nitriding rate for the entire set of nanocrystallites is expressed by the following equation [46–49]:

$$r = k(S_{sp} - S_{pr})(P - P_0)f(\alpha) \quad (3)$$

where  $k$  is the constant of the nitriding reaction rate,  $S_{sp}$  is the specific surface area,  $S_{pr}$  is the surface occupied by promoters,  $P$  is the current nitriding potential, and  $f(\alpha)$  is the conversion degree function.

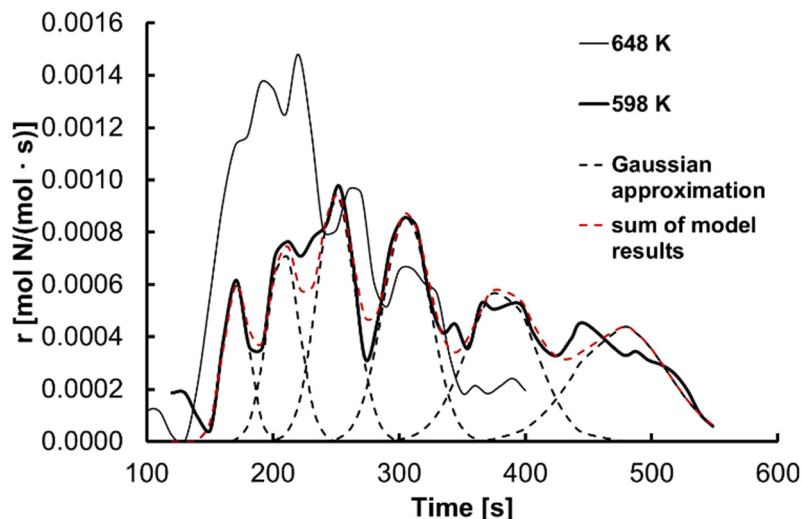


**Figure 2.** Dependence of the nitriding rate of nanocrystalline iron at 598 and 648 K on time. The red dashed line indicates the total reaction rate resulting from the proposed model.

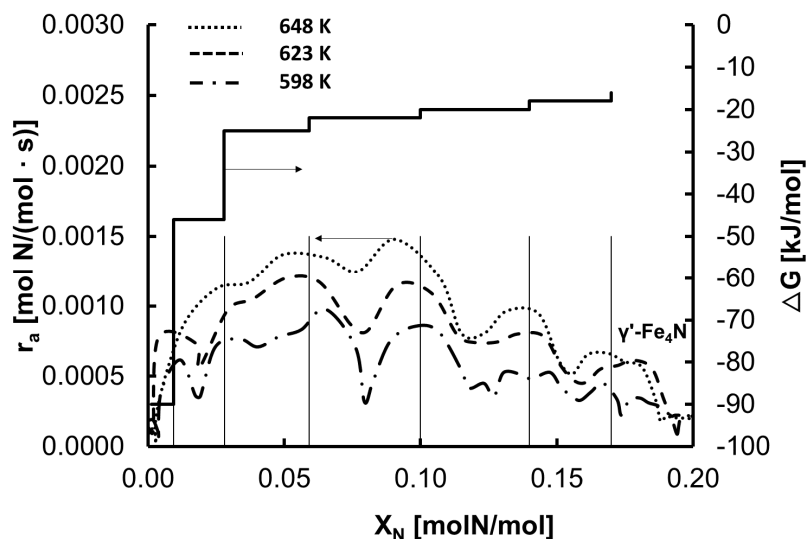


**Figure 3.** Dependence of the nanocrystalline iron nitriding rate and free enthalpy of nitrogen segregation to the nanocrystalline iron surface on the concentration of nitrogen in the solid sample.

For a single nanocrystallite of a medium size, the nanocrystalline iron nitriding process with ammonia was modeled numerically. The nitriding rate of this nanocrystallite is expressed as follows:

$$r_i = k (S_{sp} - S_{pr})_i (1 - \theta_i) f(P)_i \tag{4}$$

where  $(S_{sp} - S_{pr})$  is the specific active surface area of nanocrystallite,  $\theta$  is the active surface coverage degree, and the subscript  $i$  represents the  $i$ -th nanocrystallite.

The above equation is valid for the range of  $0 < X_N < X_N^{cri}$ .

In nanomaterials, the diffusion path of nitrogen in the volume of nanocrystallites is very short, so the concentration in the volume is close to the equilibrium values. There is

little difference between the potential of nitrogen adsorbed on the surface of the solid ( $\mu_s$ ) and that dissolved in the solid's volume ( $\mu_b$ ):

$$\mu_g = \mu_s \approx \mu_b \quad (5)$$

In this case, the nitriding process rate is not limited by the adsorption process rate. Chemical equilibrium between the substance adsorbed on the nanocrystallite surface and that dissolved in its volume can be described by McLean–Langmuir equation [50]:

$$\frac{KP}{1 - KP} = \frac{\gamma X_b}{1 - \gamma X_b} \exp\left(\frac{-\Delta G}{RT}\right) \quad (6)$$

where  $\Delta G$  is the free enthalpy of segregation of a substance,  $R$  is the gas constant,  $\gamma$  is the activity coefficient, and  $X_b$  is the nitrogen molar concentration.

Fowler and Guggenheim proposed [51] that the dependence of the free enthalpy of segregation ( $\Delta G(X_b)$ ) on the concentration of substance ( $X_b$ ) in the nanocrystallite is linear, and is valid for one phase (stable according to the Fe–N thermodynamic system):

$$\Delta G(X_b) = \Delta G_0 + \alpha X_b \quad (7)$$

where  $\alpha$  is the proportionality coefficient.

In the state of chemical equilibrium, when the chemical potential of nitrogen is equal to the absolute value of the potential change in the deformed crystal lattice of nanocrystalline iron, the saturated solution of  $\alpha$ -Fe(N)—which is in a state of chemical equilibrium—is transformed to an unsaturated solution of nitrogen in the  $\gamma$ -iron crystallographic phase—which, in turn, is in a state of transition—and further to  $\gamma'$ -Fe<sub>4</sub>N nitride, which is again in the chemical equilibrium state [18,19]. The step change in the nanocrystalline iron nitriding rate (Figures 2 and 3) can be explained by the gradual change in the degree of coverage of the iron surface with nitrogen (Figure 4), caused by the gradual change in the free enthalpy of nitrogen segregation (Figure 3). At each step change, a metastable state of FeN<sub>x</sub> is formed. Therefore, the continuous function (Equation (6)) was modified to a stepwise variable function. Transformation of a single  $\alpha$ -Fe(N) nanocrystallite into  $\gamma'$ -Fe<sub>4</sub>N occurs via the formation of six metastable FeN<sub>x</sub> states. In the first stage of the nitriding process, a solution of nitrogen in nanocrystalline iron— $\alpha$ -Fe(N)—is obtained, for which the free enthalpy of segregation equals  $-90$  kJ/mol [52]. From the stable phase of  $\alpha$ -Fe(N), after exceeding a critical concentration of ca.  $X_N = 0.004$  mol N/mol, a metastable phase is formed, where maximum coverage of the surface with nitrogen is reached at a critical  $X_N$  value for the metastable phase after surface coverage is increased by an increase in the concentration of nitrogen in the nanocrystallite volume. Figure 4 shows the dependence of the coverage of the iron surface with nitrogen and the concentration of nitrogen in volume on the nitriding potential. The value of the minimum nitriding potential at which the phase transformation in the nitriding reaction starts from nanocrystalline iron to iron nitrides is taken from Figure 1. With the minimum nitriding potential  $P_0 = 0.034$  Pa<sup>-0.5</sup>, the degree of surface coverage of a single iron nanocrystallite— $\alpha$ -Fe(N)—with nitrogen is  $\theta \approx 0.999$  (for  $\Delta G = -90$  kJ/mol). Changes in the surface coverage during the single iron nanocrystallite nitriding process for subsequent metastable phase transformations at 598 K were calculated based on Equations (4) and (6). Based on Equation (7), values of the free enthalpy of segregation were calculated, and the results are shown in Figure 3 in relation to the nitrogen concentration in iron.

The measured rate of the reaction is the sum of the process rates for a given set of nanocrystallites in the sample, as follows:

$$r = \sum_{i=1}^{i=n} r_i \quad (8)$$

According to Equation (4), the nitriding reaction rate is a function of the nanocrystallites' specific active surface area distribution [46–49]. The maximum rate of formation of individual metastable phases corresponds to the maximum of the specific active surface area distribution of nanocrystallites. Assuming that the crystallites' specific active surface area distribution is normal (Gaussian), Figure 2 shows the dependence of the nanocrystalline iron nitriding rate on time, on which the subsequent transformations of the metastable phases are marked. For such a distribution, the maximum corresponds to the average specific active surface area of the nanocrystallites. The critical nitrogen concentrations in iron nanocrystallites corresponding to the maximum rate of formation of the six metastable phases are 0.01, 0.03, 0.06, 0.10, 0.14, and 0.17 mol N/mol, respectively. Determined values are indicated by vertical lines in Figure 3.

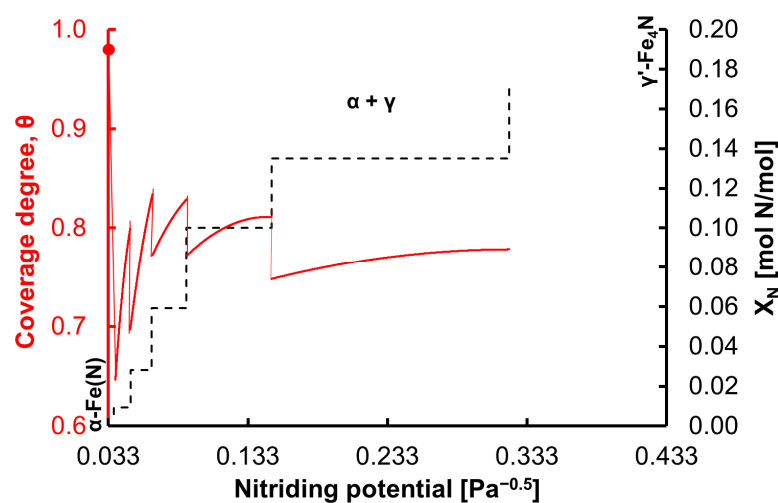


**Figure 4.** Dependence of coverage of the iron surface with nitrogen and concentration of nitrogen in the iron nanocrystallite volume on the nitriding potential.

## 5. Conclusions

In the nitriding process of nanocrystalline iron in an ammonia atmosphere, six oscillating changes in the nitriding rate of nanocrystalline iron were observed. The oscillations depended on the concentration of nitrogen in the solid sample. The oscillations occurring during the nitriding of nanocrystalline iron are related to the specific active surface area distribution of nanocrystallites, as well as to the formation of metastable nitrides. The observed transition between stable phases is caused by step changes in the free enthalpy of segregation, resulting in phase changes.

**Author Contributions:** Conceptualization, W.A.; methodology, K.S. and R.P.; validation, W.A., K.S. and R.P.; formal analysis, K.S. and Z.L.-B.; investigation, K.S. and R.P.; data curation, W.A.; writing—original draft preparation, K.S. and R.P.; writing—review and editing, W.A., R.P. and Z.L.-B.; visualization, K.S. and R.P.; supervision, W.A.; project administration, W.A.; funding acquisition, W.A. All authors have read and agreed to the published version of the manuscript.

**Funding:** This research and APC were funded by The National Science Centre, Poland, grant number 2017/27/B/ST8/02947.

**Institutional Review Board Statement:** Not applicable.

**Informed Consent Statement:** Not applicable.

**Acknowledgments:** The scientific work was financed by The National Science Centre, Poland, under the program “Opus”, project no. 2017/27/B/ST8/02947.

**Conflicts of Interest:** The authors declare no conflict of interest.

## References

1. Love, K.S.; Emmett, P.H. The Catalytic Decomposition of Ammonia over Iron Synthetic Ammonia Catalysts. *J. Am. Chem. Soc.* **1941**, *63*, 3297–3308. [[CrossRef](#)]
2. Logan, S.R.; Moss, R.L.; Kemball, C. The Catalytic Decomposition of Ammonia on Evaporated Iron Films. *Trans. Faraday Soc.* **1958**, *54*, 922–930. [[CrossRef](#)]
3. Grabke, H.J. Reaction of Ammonia, Nitrogen, and Hydrogen on the Surface of Iron. II. Kinetics of Iron Nitridation with Nitrogen and Nitrogen Desorption. *Ber. Bunsenges. Phys. Chem.* **1968**, *4*, 533–543.
4. Grabke, H.J. Kinetics of Nitriding Iron as a Function of the Oxygen Activity of the Gas. *Arch. Eisenhüttenwes.* **1973**, *44*, 603–608.
5. Inokuti, Y.; Nishida, N.; Ohashi, N. Formation of Fe<sub>3</sub>N, Fe<sub>4</sub>N and Fe<sub>16</sub>N<sub>2</sub> on the Surface of Iron. *Metall. Trans. A* **1975**, *6*, 773–784. [[CrossRef](#)]
6. Arabczyk, W.; Wróbel, R. Study of the Kinetics of Nitriding of Nanocrystalline Iron Using TG and XRD Methods. *Solid State Phenom.* **2003**, *94*, 185–188. [[CrossRef](#)]
7. Arabczyk, W.; Pelka, R. Studies of the Kinetics of Two Parallel Reactions: Ammonia Decomposition and Nitriding of Iron Catalyst. *J. Phys. Chem. A* **2009**, *113*, 411–416. [[CrossRef](#)]
8. Arabczyk, W.; Zamłyński, J.; Moszyński, D. Kinetics of Nanocrystalline Iron Nitriding. *Pol. J. Chem. Technol.* **2010**, *12*, 38–43. [[CrossRef](#)]
9. Pelka, R.; Arabczyk, W. Modelling of Nanocrystalline Iron Nitriding Process — Influence of Specific Surface Area. *Chem. Pap.* **2011**, *65*, 198–202. [[CrossRef](#)]
10. Moszyński, D. Nitriding of Nanocrystalline Iron in the Atmospheres with Variable Nitriding Potential. *J. Phys. Chem. C* **2014**, *118*, 15440–15447. [[CrossRef](#)]
11. Arabczyk, W.; Wróbel, R. Utilisation of XRD for the Determination of the Size Distribution of Nanocrystalline Iron Materials. *Solid State Phenom.* **2003**, *94*, 235–238. [[CrossRef](#)]
12. Wróbel, R.; Arabczyk, W. Solid-Gas Reaction with Adsorption as the Rate Limiting Step. *J. Phys. Chem. A* **2006**, *110*, 9219–9224. [[CrossRef](#)] [[PubMed](#)]
13. Moszyńska, I.; Moszyński, D.; Arabczyk, W. Hysteresis in Nitriding and Reduction in the Nanocrystalline Iron-Ammonia-Hydrogen System. *Przem. Chem.* **2009**, *88*, 526–529.
14. Moszyński, D.; Moszyńska, I.; Arabczyk, W. Iron Nitriding and Reduction of Iron Nitrides in Nanocrystalline Fe-N System. *Mater. Lett.* **2012**, *78*, 32–34. [[CrossRef](#)]
15. Wilk, B.; Arabczyk, W. Studies on the Nitriding and Reduction in the Nanocrystalline Iron-Ammonia-Hydrogen System. *Przem. Chem.* **2014**, *93*, 1036–1040.
16. Wilk, B.; Arabczyk, W. Investigation of Nitriding and Reduction Processes in a Nanocrystalline Iron–Ammonia–Hydrogen System at 350 °C. *Phys. Chem. Chem. Phys.* **2015**, *17*, 20185–20193.
17. Wilk, B.; Kiełbasa, K.; Arabczyk, W. Nitriding of Nanocrystalline Iron with Ammonia–Hydrogen Mixture at 300 °C. *Przem. Chem.* **2015**, *94*, 1816–1820.
18. Arabczyk, W.; Ekiert, E.; Pelka, R. Size-Dependent Transformation of  $\alpha$ -Fe into  $\gamma'$ -Fe<sub>4</sub>N in Nanocrystalline the Fe–NH<sub>3</sub>–H<sub>2</sub> System. *J. Phys. Chem. C* **2016**, *120*, 17989–17995. [[CrossRef](#)]
19. Arabczyk, W.; Ekiert, E.; Pelka, R. Hysteresis Phenomenon in a Reaction System of Nanocrystalline Iron and a Mixture of Ammonia and Hydrogen. *Phys. Chem. Chem. Phys.* **2016**, *18*, 25796–25800. [[CrossRef](#)]
20. Arabczyk, W.; Narkiewicz, U.; Moszyński, D. Double-Layer Model of the Fused Iron Catalyst for Ammonia Synthesis. *Langmuir* **1999**, *15*, 5785–5789. [[CrossRef](#)]
21. Moszyński, D.; Kiełbasa, K.; Arabczyk, W. Influence of Crystallites' Size on Iron Nitriding and Reduction of Iron Nitrides in Nanocrystalline Fe-N System. *Mater. Chem. Phys.* **2013**, *141*, 674–679. [[CrossRef](#)]
22. Moszyński, D.; Moszyńska, I.; Arabczyk, W. The Transformation of  $\alpha$ -Fe into  $\gamma'$ -Fe<sub>4</sub>N in Nanocrystalline Fe-N System: Influence of Gibbs–Thomson Effect. *Appl. Phys. Lett.* **2013**, *103*, 253108. [[CrossRef](#)]
23. Moszyński, D.; Moszyńska, I. Phase Transformations during Nitriding of Nanocrystalline Iron. *Przem. Chem.* **2013**, *92*, 1332–1335.
24. Lehrer, E. The Equilibrium Iron-Hydrogen-Ammonia. *Z. Electrochem.* **1930**, *36*, 383–392.
25. Hugo, P. Stabilität und Zeitverhalten von Durchfluß—Kreislauf—Reaktoren. *Ber. Bunsenges.* **1970**, *74*, 121–127.
26. Ertl, G. *Handbook of Heterogeneous Catalysis*; Wiley: Weinheim, Germany, 2008; p. 1492.
27. Ertl, G. *Reactions at Solid Surfaces*; Wiley: Hoboken, NJ, USA, 2009; p. 159.
28. Ertl, G. Temporal and Spatial Self-Organization in Catalysis at Single Crystal Surfaces. *Catal. Lett.* **1991**, *9*, 219–230. [[CrossRef](#)]
29. Eiswirth, M.; Schwankner, R.; Ertl, G. Conditions for the Occurrence of Kinetic Oscillations in the Catalytic Oxidation of CO on a Pt(100) Surface. *Z. Phys. Chem. Neue Fol.* **1985**, *144*, 59–67. [[CrossRef](#)]
30. Schwankner, R.J.; Eiswirth, M.; Moller, P.; Wetzl, K.; Ertl, G. Kinetic Oscillations in the Catalytic CO Oxidation on Pt(100): Periodic Perturbations. *J. Chem. Phys.* **1987**, *87*, 742–749. [[CrossRef](#)]
31. Eiswirth, R.M.; Krischer, K.; Ertl, G. Nonlinear Dynamics in the CO-Oxidation on Pt Single Crystal Surfaces. *Appl. Phys. A* **1990**, *51*, 79–90. [[CrossRef](#)]
32. Vilyunov, V.N.; Ryabinin, V.K. Oscillations in the Burning of Hydrogen in a Well-Stirred Reactor at Low Pressures. *Combust. Explos. Shock* **1991**, *27*, 203–211. [[CrossRef](#)]

33. Chakrabarty, T.; Hudgins, R.R.; Silveston, P.L. Spontaneous, Random Oscillations in the Rate of CO Oxidation over Pt/Alumina. *Can. J. Chem. Eng.* **1987**, *65*, 693–695.
34. Hu, Y.H.; Rückenstein, E. Catalyst Temperature Oscillations during Partial Oxidation of Methane. *Ind. Eng. Chem. Res.* **1998**, *37*, 2333–2335. [[CrossRef](#)]
35. Gorodetskii, V.V.; Drachsel, W. Kinetic Oscillations and Surface Waves in Catalytic CO + O<sub>2</sub> Reaction on Pt Surface: Field Electron Microscope, Field Ion Microscope and High Resolution Electron Energy Loss Studies. *Appl. Catal. A-Gen.* **1999**, *188*, 267–275. [[CrossRef](#)]
36. Bzovska, I.S.; Mryglod, I.M. Chemical Oscillations in Catalytic CO Oxidation Reaction. *Condens. Matter Phys.* **2010**, *13*, 34801. [[CrossRef](#)]
37. Berlowitz, P.J.; Peden, C.H.F.; Goodman, D.W. Kinetics of Carbon Monoxide Oxidation on Single-Crystal Palladium, Platinum, and Iridium. *J. Phys. Chem.* **1988**, *92*, 5213–5221. [[CrossRef](#)]
38. Ivanova, E.A.; Chumakova, N.A.; Chumakov, G.A.; Boronin, A.I. Modeling of Relaxation Oscillations in CO Oxidation on Metallic Catalysts with Consideration of Reconstructive Heterogeneity of the Surface. *Chem. Eng. J.* **2005**, *107*, 191–198. [[CrossRef](#)]
39. Lashina, E.A.; Slavinskaya, E.M.; Chumakova, N.A.; Stonkus, O.A.; Gulyaev, R.V.; Stadnichenko, A.I.; Chumakov, G.A.; Boronin, A.I.; Demidenko, G.V. Self-Sustained Oscillations in CO Oxidation Reaction on PdO/Al<sub>2</sub>O<sub>3</sub> Catalyst. *Chem. Eng. Sci.* **2012**, *83*, 149–158. [[CrossRef](#)]
40. van Neer, F.; Blied, A. The Feedback Mechanism in Self-Oscillations for CO Oxidation over EUROPT-3. *Chem. Eng. Sci.* **1999**, *54*, 4483–4499. [[CrossRef](#)]
41. Makeev, A.G.; Semendyaeva, N.L.; Slinko, M.M. Synergetic Effect and Oscillatory Behavior of CO Oxidation over a Bimetallic Composite Catalyst. *Chem. Eng. J.* **2015**, *282*, 3–10. [[CrossRef](#)]
42. Saraev, A.A.; Vinokurov, Z.S.; Kaichev, V.V.; Shmakov, A.N.; Bukhtiyarov, V.I. The Origin of Self-Sustained Reaction-Rate Oscillations in the Oxidation of Methane over Nickel: An Operando XRD and Mass Spectrometry Study. *Catal. Sci. Technol.* **2017**, *7*, 1646–1649. [[CrossRef](#)]
43. Skulmowska, K.; Pelka, R.; Arabczyk, W. Oscillatory Kinetics in the Process of Reduction of Nanocrystalline Iron Nitride  $\gamma'$ -Fe<sub>4</sub>N. *J. Phys. Chem. C* **2017**, *121*, 14712–14716. [[CrossRef](#)]
44. Arabczyk, W.; Jasińska, I.; Lubkowski, K. The Surface Properties of Iron Catalyst for Ammonia Synthesis. *React. Kinet. Catal. Lett.* **2004**, *83*, 385–392. [[CrossRef](#)]
45. Kunze, J. *Nitrogen and Carbon in Iron and Steel Thermodynamics*; Akademie-Verlag: Berlin, Germany, 1990.
46. Pelka, R.; Arabczyk, W. Studies of the Kinetics of Reaction between Iron Catalysts and Ammonia—Nitriding of Nanocrystalline Iron with Parallel Catalytic Ammonia Decomposition. *Top. Catal.* **2009**, *52*, 1506–1516. [[CrossRef](#)]
47. Arabczyk, W.; Pelka, R.; Wilk, B. Studies of Phase Transitions Occurring in the System of Nanocrystalline Fe/NH<sub>3</sub>/H<sub>2</sub>. *Mater. Chem. Phys.* **2019**, *237*, 121853.
48. Ekiert, E.; Wilk, B.; Lenzion-Bieluń, Z.; Pelka, R.; Arabczyk, W. Study of Phase Transitions Occurring in a Catalytic System of ncFe-NH<sub>3</sub>/H<sub>2</sub> with Chemical Potential Programmed Reaction (CPPR) Method Coupled with In Situ XRD. *Catalysts* **2021**, *11*, 183. [[CrossRef](#)]
49. Arabczyk, W.; Pelka, R.; Jasińska, I.; Lenzion-Bieluń, Z. Reaction Model Taking into Account the Catalyst Morphology and Its Active Specific Surface in the Process of Catalytic Ammonia Decomposition. *Materials* **2021**, *14*, 7229. [[CrossRef](#)] [[PubMed](#)]
50. Benard, J. Chapter 9 Composition of Grain Boundaries in Binary Alloys. *Stud. Surf. Sci. Catal.* **1983**, *13*, 245–270.
51. Fowler, R.H.; Guggenheim, E.A. *Statistical Thermodynamics*; Cambridge University Press: Cambridge, UK, 1939; p. 429.
52. Grabke, H.J. Conclusions on the Mechanism of Ammonia-Synthesis from the Kinetics of Nitrogenation and Denitrogenation of Iron. *Z. Phys. Chem. Neue Fol.* **1976**, *100*, 185–200. [[CrossRef](#)]